

# A Novel Low-RCS and Wideband Circularly Polarized Patch Array Based on Metasurface

Xue-wen ZHU<sup>1</sup>, Jun GAO<sup>1</sup>, Xiang-yu CAO<sup>1</sup>, Tong LI<sup>1</sup>,  
Yue-jun ZHENG<sup>1</sup>, Li-li CONG<sup>1</sup>, Liao-ri JI-DI<sup>1</sup>, Bo-wen ZHU<sup>2</sup>

<sup>1</sup>Information and Navigation Institute of Air Force Engineering University, Xi'an, Shaanxi, 710077, China

<sup>2</sup>Armed Police Engineering University, Xi'an, Shaanxi, 710038, China

zhuxiaoshuai4088@163.com

Submitted April 7, 2018 / Accepted November 12, 2018

**Abstract.** In this paper, a novel circularly polarized (CP) array antenna based on metasurface (MS) is designed to realize wideband radar cross section (RCS) reduction, wideband operation and high gain. The MS is composed of compact polarization-dependent artificial magnetic conductors (PDAMCs), by regularly arranging the PDAMCs like chessboard directly on the top of the patch antenna, the MS can significantly bring RCS down. On the other hand, due to the compact structure of MS and the driven array patches, surface wave propagates on the MS and generates additional resonances to achieve wide operation band and high gain. Both the simulated and measured results indicate that the RCS at bore-sight is reduced more than 6 dB from 5.08 GHz to 11.46 GHz (77.15%) except for some frequency points. The antenna yielded a good broadside left-hand CP radiation, the  $|S_{11}| < -10$  dB impedance bandwidth is from 5.03 GHz to 7.4 GHz (38.13%) and the 1-dB axial ratio bandwidth is from 4 GHz to 8 GHz. Both the radiating and scattering performances have been obviously improved.

## Keywords

Low RCS, high-gain, wideband, metasurface antenna

## 1. Introduction

Circularly polarized patch antennas [1–3] have been widely applied in modern communication due to their excellent advantages of low profile, easy fabrication, stability and reliability against multipath/fading communication environment. However, traditional designs of CP antennas mainly suffer the problems of narrow operation band and low gain. In order to solve these problems, many alternative engineering methods have been researched and applied. In [4], a novel CP antenna composed of  $2 \times 2$  H-shaped patches is designed to realize the  $|S_{11}| < -10$  dB impedance bandwidth of 85% and the 3-dB axial-ratio bandwidth of 89% for employing metamaterial transmis-

sion-lines as feeding network. In [5], a cost-effective solution for the performance enhancement of circularly polarized array antennas by using a thin metasurface is proposed. Son Xuat Ta and Ikmo Park have designed a  $2 \times 2$  element array based on circularly polarized metasurface-based antennas fed by a sequential phase network, which can realize the  $|S_{11}| < -10$  dB impedance bandwidth from 7.5 to 11 GHz and the 3-dB AR bandwidth from 8.4 to 10.7 GHz [6].

However, with the urgent demand of stealth technology applied in military communication, RCS-reduction has been an important research subject. It is well known that antennas play an important role in transmitting and receiving message, but also are one of the main contributors to the overall RCS of platforms. The radiating apertures of the above works make a contribution to RCS-improvement of the whole platform. Conventional ways can significantly bring RCS down but deteriorate radiating performance. It has been a long period for researchers to solve the problem of reducing RCS while maintaining or enhancing the radiation performance. Recently, MS has received popular attention for light weight, low profile, ease of fabrication, extraordinary electromagnetic behavior, such as frequency selective surface (FSS) [7], [8], artificial magnetic conductors (AMC) [9–11], electromagnetic band-gap (EBG) [12], [13], polarization rotation metasurface (PRMS) [14] and perfect metamaterial absorber [15], [16]. In [7], the MS composed of new FSS units is applied as a superstrate on the original microstrip antenna to realize wideband RCS reduction and gain enhancement, but the operation-band is from 10.74–12.33 GHz (about 13.8%). In [8], a novel FSS superstrate is put on a new circularly polarized patch antenna to achieve low RCS and high gain, but the operation band of the circularly polarized antenna is from 12.32–13.08 GHz and 12.31–13.22 GHz (7.3%) and the profile is much high. In [10], different sizes of unit cells are arranged on a microstrip antenna array for ultra-wideband RCS reduction while the radiation performance is preserved not enhanced. In [17], a broadband low-RCS circularly polarized array using metasurface is designed, the antenna achieves  $-10$ dB impedance bandwidth of 17%

with a high profile. According to the previous analysis of the mentioned works, the low-profile MS applied on the wideband circularly polarized antennas to reduce RCS while enhance radiating performance is barely studied for the structure of low-RCS MS will influence the propagation of radiating waves.

In this paper, a novel low profile, low RCS, wideband operation CP patch array based on MS is designed. The array is composed of  $2 \times 2$  elements, each element contains a truncated corner driven patch which sandwiches between the MS and ground with a coaxial feed of  $0^\circ, 90^\circ, 180^\circ$  and  $270^\circ$ , respectively. Each MS element consists of a lattice of  $4 \times 4$  periodic PDAMCs units, by arranging PDAMCs like a chessboard directly on the top of the patch array. When illuminated by the radar detecting wave, the MS produces broadband reflection cancellation in order to reduce RCS at the bore-sight. On the other hand, the compact structure of MS allows the radiating electromagnetic waves propagate on the MS to generate additional resonances to widen the operation band. Both the simulated and measured results indicate that the radar cross section (RCS) at the bore-sight is reduced more than 6 dB from 5.08 GHz to 11.46 GHz except for some frequency points. The array antenna has a good broadside left-hand CP radiation, with the  $|S_{11}| < -10$  dB impedance bandwidth from 5.03 to 7.4 GHz and the 1-dB axial ratio bandwidth of 4–8 GHz. Both the radiating and scattering performances are improved well.

## 2. RCS-reduction Mechanism and Design of PDAMC Unit

The RCS reduction mechanism of AMC is reflected energy cancellation by controlling the reflection phases to achieve the low reflected magnitude at bore-sight, which results in the dispersion of the backscattering energy. Traditional RCS-reduction methods are the combination of periodic perfect electric conductor (PEC) and AMC, but suffer from narrow RCS-reduction band. After that, different sizes or structures of AMC units have been designed to expand the bandwidth of RCS-reduction [10].

In 2009, Fan Yang [19], [20] put forward a new structure of EBG, which is sensitive to polarized wave called polarization-dependent electromagnetic band gap (PDEBG). After that, polarization-dependent artificial magnetic conductors (PDAMCs) have been widely researched [21], [22]. According to the concept of standard array theory [17], [11], by regularly arranging PDAMC units and the identical ones with a rotating phase of  $90^\circ$  like a chessboard as shown in Fig. 1, the RCS at bore-sight can be significantly reduced. The total reflection can be represented by:

$$\mathbf{E}_r = \mathbf{E}_{AMC1} \cdot F_1 + \mathbf{E}_{AMC2} \cdot F_2 \quad (1)$$

$F_1, F_2$  are the array factors.  $\mathbf{E}_{AMC1}, \mathbf{E}_{AMC2}$  are the reflection fields of x-oriented and y-oriented PDAMCs respectively, which can also be replaced by:

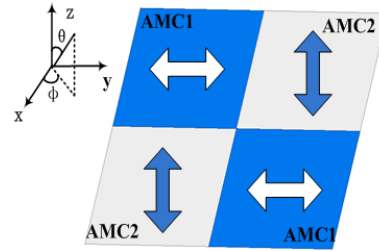


Fig. 1. The RCS reduction mechanism of energy cancellation.

$$\begin{cases} \mathbf{E}_{AMC1} = \mathbf{E}_1 e^{j\varphi_1} \cdot \mathbf{E}_{unit1} \\ \mathbf{E}_{AMC2} = \mathbf{E}_2 e^{j\varphi_2} \cdot \mathbf{E}_{unit2} \end{cases} \quad (2)$$

When illuminated by the plane wave, it can be concluded that  $F_1 = F_2 = 1$ . In order to simplify the equation, we assume that  $\mathbf{E}_1 \mathbf{E}_{unit1} = \mathbf{E}_2 \mathbf{E}_{unit2} = \mathbf{A}$ , equation (1) can be replaced by:

$$\mathbf{E}_r = \mathbf{A} e^{j\varphi_1} (1 + e^{j(\varphi_2 - \varphi_1)}) \quad (3)$$

where  $\varphi_1$  is the reflection phase of x-polarized PDAMC while  $\varphi_2$  is the reflection phase of y-pol. When  $|\varphi_1 - \varphi_2| = 180^\circ$ , the reflection wave can be totally canceled out. Usually a 10-dB RCS-reduction is set of the standard whether the antenna can effectively reduce RCS. Here comes another equation:

$$\log_{10} \left( \frac{|\mathbf{E}_r|^2}{|\mathbf{E}_{pec}|^2} \right) \leq -10 \text{ dB} \quad (4)$$

where  $\mathbf{E}_{pec}$  is the reflection of the same size PEC unit under the same environment. It can be calculated that:

$$143^\circ \leq D\text{-value} = |\varphi_2 - \varphi_1| \leq 217^\circ. \quad (5)$$

For further simplification,  $D\text{-value}$  between  $150^\circ \sim 210^\circ$  was set as an effective phase difference.

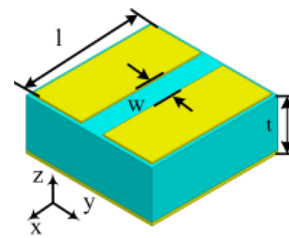


Fig. 2. Geometry of the proposed PDAMC unit.

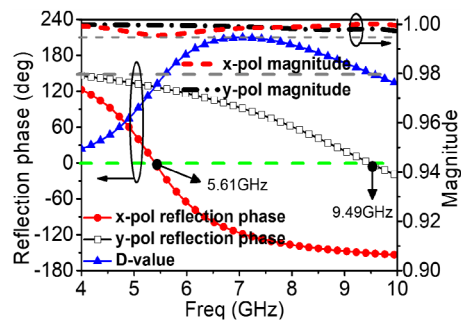


Fig. 3. Reflection response of the unit.

According to the RCS-reduction mechanism, this paper designs a novel PDAMC unit as shown in Fig. 2. The top layer is a square patch with a stripe slot on the x-direction, while the bottom layer is a whole metallic patch. The substrate is made of F4B-2 ( $\epsilon_r = 2.65$ ,  $\tan\delta = 0.001$ ) with the size of  $a = 8 \text{ mm} \times a = 8 \text{ mm} \times t = 3 \text{ mm}$ . Figure 3 gives the simulated reflection response of the unit under x-polarization and y-pol incidence wave. It can be concluded that the magnitudes of both polarizations maintain upon 0.993 mm from 4 GHz to 10 GHz, which indicates that the incident wave is almost reflected with nearly absorption. For the structure of unit is unsymmetrical, the reflection phase shows obvious dependence to the polarization of incidence wave. The zero value of x-polarization appears at 5.61 GHz, while that of y-polarization appears at 9.49 GHz. The D-value between  $150^\circ \sim 210^\circ$  is from 5.66 GHz to 9.45 GHz that the RCS can be reduced at least 10 dB.

To explain the phenomenon, it is well known that PDAMC can be seemed as an equivalent LC circuit and the resonating frequency point is mainly affected by the value of  $1/(2\pi\sqrt{LC})$ , while the reflective phase is zero. The length of the patches is related to the inductive component L while the gap between adjacent patches is related to the capacitive element C. For the structure of the unit is unsymmetrical, the resonating frequency appears differently under x-pol and y-pol incidence wave. Figure 4 shows the E-field distribution at 5.61 GHz and 9.49 GHz under x-pol and y-pol incidence wave. At 5.61 GHz, the patch resonates strongly under the x-pol plane wave. The E-field mainly concentrates at the two ends along the x-axis while that of y-axis is much less. Therefore, the zero value of x-polarization appears at 5.61 GHz. At 9.49 GHz, the patch resonates strongly under the y-pol plane wave. The E-field mainly concentrates at the two ends along the y-axis while that of x-axis is much less. Therefore, the zero value of y-polarization appears at 9.49 GHz. The above analysis proves the exactness of the equivalent LC circuit.

In order to verify the statement of equivalent LC circuit and observe the maximum bandwidth for phase cancellation, here we set  $w = 1.4 \text{ mm}$  and change the value of  $l$ , Figure 5(a) gives the reflection phases of the x-pol and y-pol incidence. It can be concluded that the value of  $l$  mainly influences the resonating points of the x-polarized incidence. With the increasing of  $l$ , the zero points of both

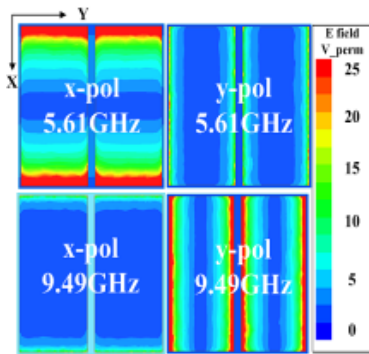


Fig. 4. E-field distribution of the PDAMC unit.

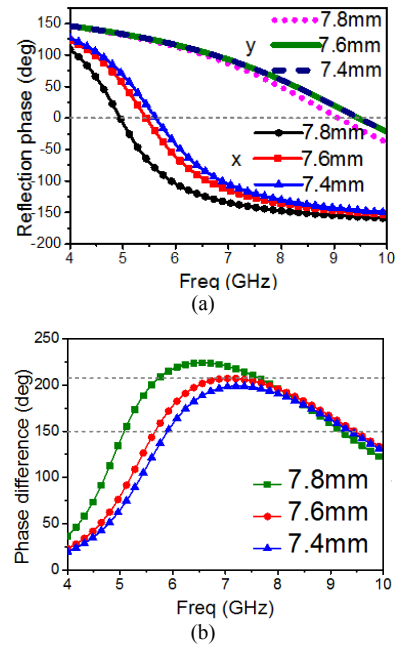


Fig. 5. Reflection response with change of  $l$ . (a) Reflection phase of the unit. (b) D-value.

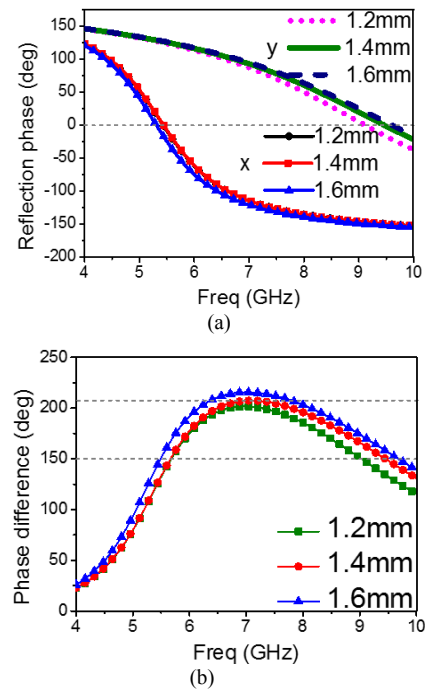


Fig. 6. Reflection response with change of  $w$ . (a) Reflection phase of the unit. (b) D-value.

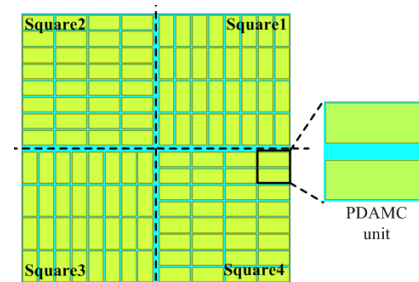


Fig. 7. Geometry of the proposed MS.

x-pol and y-pol move to the low frequency for the increasing of the inductive components  $L$ . And as shown in Fig. 5(b), when  $l = 7.6$  mm, the bandwidth of the phase difference between the  $180^\circ \pm 30^\circ$  is broader than other values. Next we set  $l = 7.6$  mm and change the value of  $w$ . As shown in Fig. 6(a), similar to what is analyzed before, the value of  $w$  mainly influences the resonating points of the y-pol incident wave. With the increasing of  $w$ , the zero points of both x-pol and y-pol move to the low frequency for the increasing of the capacitive elements  $C$ . And as shown in Fig. 6(b), when  $w = 1.4$  mm, the bandwidth of the phase difference between the  $180^\circ \pm 30^\circ$  is broader than other values. According to the pervious parameters optimization, we get the optimal parameters for  $l = 7.6$  mm,  $w = 1.4$  mm which satisfy the desired phase difference.

In order to verify the analysis of PDAMC unit, the MS is simulated in HFSS 14.0 which is composed of 4 squares as shown in Fig. 7. Each square of the MS consists of  $4 \times 4$  PDAMC units. The PDAMC units in the first and third squares have a  $90^\circ$  rotation which are different from the ones in the second and fourth squares. Figure 8 gives the simulated RCS curves of the MS and the same size of the metal plane for comparison under x-polarization wave. The measured 6-dB reduction for the x-polarized of the MS antenna occurs from 5.32 to 8.92 GHz and from 10.16 to 10.96 GHz, the maximum reductions of 27.78 dB and 26.52 dB appear at 6.72 GHz and 7.96 GHz respectively, which are in agreement with the effective phase difference band the PDAMC unit. It can be concluded that the RCS of the MS is significantly reduced compared with the metal plane.

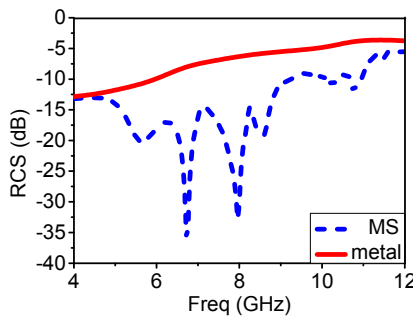


Fig. 8. Simulated RCS results of MS and metal plane.

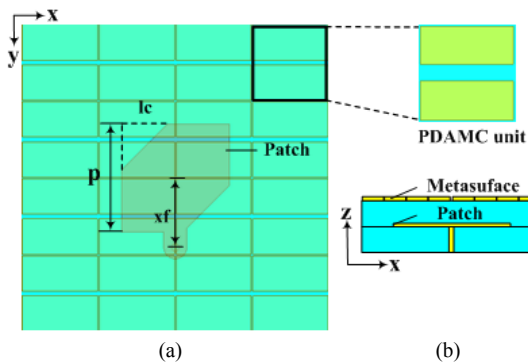


Fig. 9. Geometry of the proposed MS antenna element. (a) Top view. (b) Side view.

### 3. Design and Analysis of MS Antenna Element and MS Antenna Array

Figure 9 shows the geometry of the proposed MS antenna element which is composed of two substrates. Both substrates are made of F4B-2. The radiating patch is printed on the top surface of substrate 1 while the ground is printed on the back. The MS is printed on the upper surface of substrate 2 which is directly put on the top of substrate 1 without any gap. The MS is composed of  $4 \times 4$  PDAMCs. Figure 10 illustrates the  $S_{11}$  and gain curves comparison. The  $|S_{11}| < -10$  dB impedance bandwidth of the MS element is from 5.06 GHz to 7.74 GHz, while the reference (RF) antenna is from 6.13 GHz to 6.43 GHz. The gain curve of the MS antenna element is significantly improved compared to the RF antenna. It can be concluded that the compact structure of MS generates additional resonances for widening operation band. At the same time, the radiated electromagnetic wave spreads across the whole MS to increase the aperture for improving the radiation performance as shown in Fig. 11.

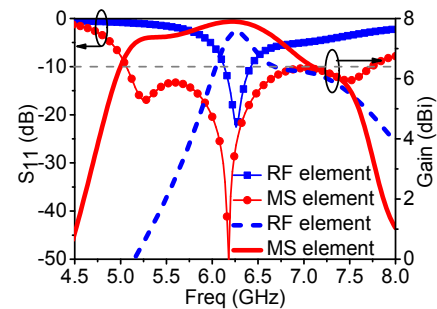


Fig. 10. The  $S_{11}$  and gain curves of the MS and RF element antennas.

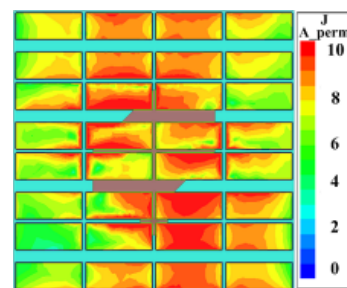


Fig. 11. Current distribution of the MS element antenna at 6.2 GHz.

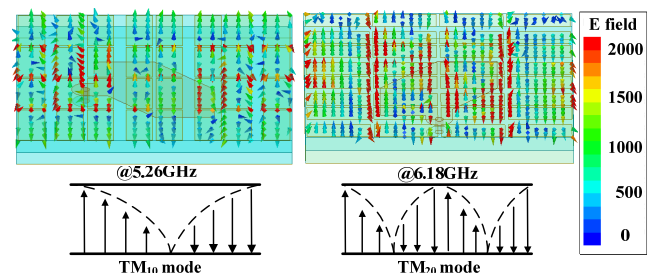


Fig. 12. E-field vector of the MS antenna element and the sketches of operating modes.

The wideband operation of MS antenna element is obtained by fusion of multiple order modes. Figure 12 gives the E-field vector of the MS antenna element and the sketches of the operating modes. At 5.26 GHz, the MS antenna element operates at  $TM_{10}$  mode which is like the operation mode of traditional microstrip antenna. At 6.18 GHz, the MS antenna element operates at  $TM_{20}$  mode. Therefore, the operation band is expanded for exciting the additional operating mode and fusing  $TM_{10}$  and  $TM_{20}$  modes.

Since the MS on the antenna element is asymmetrical which destroys the axial ratio character of the patch antenna, the MS element antenna is no longer circularly polarized but linear polarized. In order to form the CP radiation and reduce the RCS of the antenna, the designed antenna array is designed of four elements, element ②, ③, ④ are obtained by rotating the element ① with the angle of  $90^\circ$ ,  $180^\circ$ ,  $270^\circ$  as shown in Fig. 13. Port 1, 2, 3, 4 are fed with phases of  $0^\circ$ ,  $90^\circ$ ,  $180^\circ$ ,  $270^\circ$  respectively by using a phase shifter as shown in Fig. 13, so that the magnitudes radiating wave of E plane and H plane are equal but have a phase difference of  $90^\circ$  to form the circularly polarized radiation.

Since the parameters of the element are confined, to realize the compact structure and better radiation performance, the distance  $d$  between the driven patches and the  $gap$  between the elements should be further studied. As shown in Fig. 14(a), with the increase of  $d$ , the impedance bandwidth of  $|S_{11}| < -10$  dB shifts to lower frequency while the curves of gain are reduced a little in high frequency region. From Fig. 14(b), it can be concluded that with the increase of  $gap$ , the bandwidth of  $|S_{11}| < -10$  dB shifts to high frequency while the curves of gain increase a little in the high frequency region. The values of  $d$  and  $gap$  cannot be too large or small. At last, the optimal parameters value are  $d = 18.5$  mm,  $gap = 1.5$  mm. Other parameters are shown in Tab. 1.

To verify the scattering performance, the MS antenna array is exposed under the plane wave to simulate that the radar detecting wave impinges the antenna. Figure 15 gives the RCS curves of the MS and reference antenna array under x-polarization. Compared to the reference, 6-dB RCS-reduction is obtained from 5.06 GHz to 11.46 GHz except for some frequency points, the result agrees well with

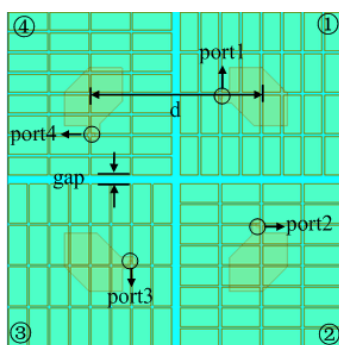


Fig. 13. Geometry of the proposed MS antenna array.

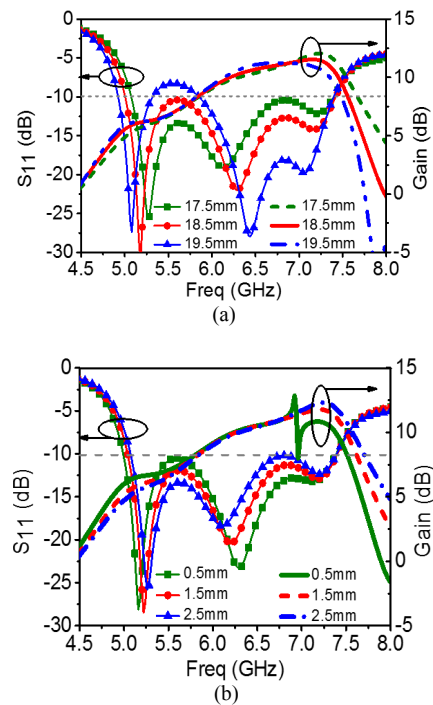


Fig. 14. The  $S_{11}$  and gain curves with change of: (a)  $d$ , (b)  $gap$ .

Parameters	$t$	$a$	$p$	$lc$	$xf$	$t_1$	$t_2$
Dimensions (mm)	3	8	14	7	8	1.5	1.5

Tab. 1. The values of other parameters.

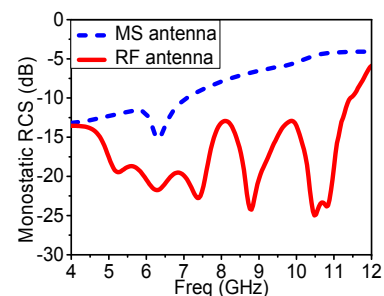


Fig. 15. The simulated monostatic RCS of the MS and RF antenna.

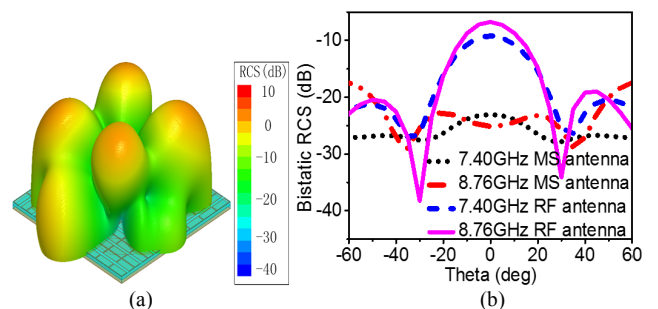


Fig. 16. RCS reduction results. (a) The 3D plot scattering pattern. (b) The bistatic RCS of the MS and RF antenna at 7.4 and 8.76 GHz.

the effective phase difference band obtained by the unit simulation. At 8.76 GHz, it achieves a maximum reduction of 18.6 dB and there exists deterioration around 8.06 GHz due to the strong coupling between the adjacent units.

Freq (GHz)	5.24	6.28	7.36
Theta range (deg)	-53.6 to 53.4	-29.2 to 29.4	-33.2 to 33.1
Maximum (dB)	7.52	6.7	13.73
Freq (GHz)	8.8	9.88	11.2
Theta range (deg)	-22.66 to 22.98	-23.2 to 23	-20.8 to 20.8
Maximum (dB)	18.38	21.18	9.18

Tab. 2. RCS reduction at different frequencies.

Figure 16(a) gives the 3D plot scattering pattern of MS antenna array under the x-pol wave at 8.76 GHz. The scattering field is distributed into four directions, and forms a low back-scattering space, that is the reason why the MS antenna has low RCS performance. Figure 16(b) gives the bistatic RCS curves of both antennas with variable thetas under x-polarized incidence at 7.4 and 8.76 GHz. It can be concluded that the RCS of MS antenna array is significantly reduced from  $-28^\circ$  to  $28^\circ$  at 7.4 GHz and from  $-60^\circ$  to  $60^\circ$  at 8.76 GHz, respectively. With the increasing of incident angle, the reduction becomes worse for that the MS is sensitive to the angle. Table 2 gives the RCS-reduction angle and reduction maximum at different frequencies, it indicates that the MS antenna array has a stable character of low RCS at bore-sight from 5.06 GHz to 11.46 GHz with the comparison of the reference antenna.

### 4. Fabrication and Measurement

For further verification, the final designed MS and RF antennas element and the MS and RF array antennas have been fabricated as shown in Fig. 17. In order to eliminate noise interference, the antennas are measured in microwave anechoic chamber using the vector network analyzer Agilent N5230C.

Figure 18 gives the simulated and measured  $S_{11}$  curves of the two antennas element. The measured  $|S_{11}| < -10$  dB impedance bandwidth of the MS element is from 5.21 GHz to 8 GHz while the simulated result is from 5.06 GHz to 7.76 GHz. The measured impedance bandwidth of the RF element is from 6.2 GHz to 6.53 GHz while the simulated result is from 6.12 GHz to 6.46 GHz. Both the measured and simulated results proved that the designed MS significantly expands the impedance bandwidth. Compared with the simulated results, the measured curves shift to the higher frequency for the fabrication and measurement tolerance.

Figure 19 gives the gain-total radiation patterns of the two element antennas at 6 GHz and 6.5 GHz. At 6 GHz, the gain of the MS element is improved by 1.77 dBi. At 6.5 GHz, the gain of the MS element is improved by 0.98 dBi. It can be explained that the gain of the MS element antenna is improved for that the radiation electromagnetic wave spreads across the whole MS. The radiation aperture is significantly expanded.

As shown in Fig. 20(a), the measured impedance band-

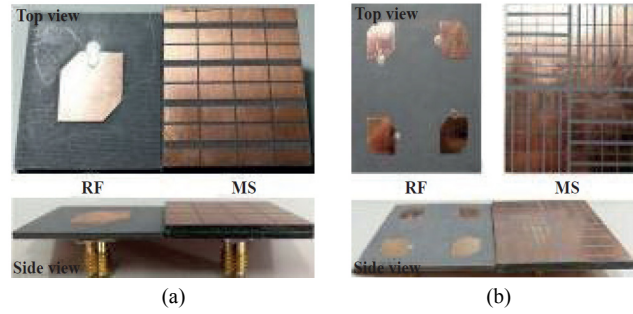


Fig. 17. Photographs of the fabricated antennas. (a) The MS and RF element antennas. (b) The MS and RF array antennas.

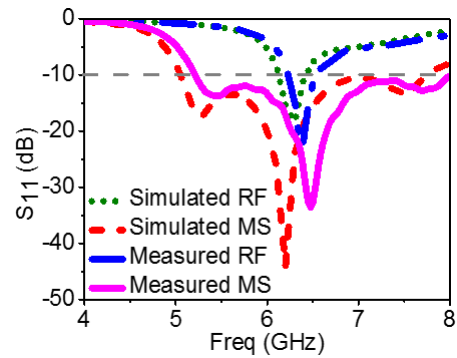


Fig. 18. The measured and simulated  $S_{11}$  curves of the RF and MS element antenna.

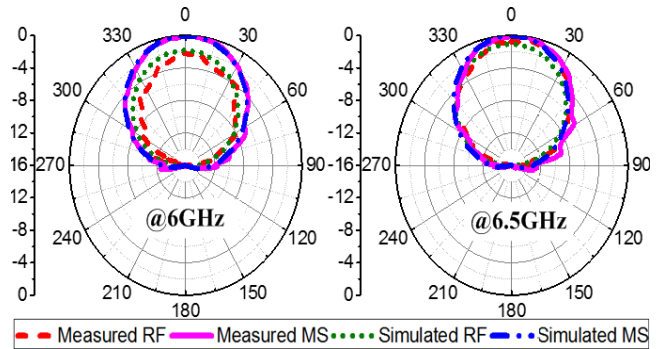


Fig. 19. Radiation patterns of the MS and RF element antennas.

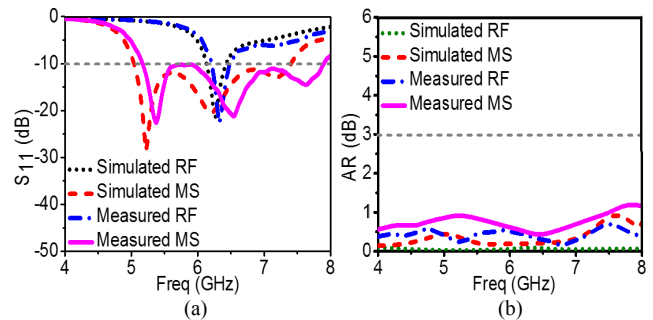


Fig. 20. The measured and simulated  $S_{11}$  and AR curves of the MS and RF antenna.

width of the MS array antenna for  $|S_{11}| < -10$  dB is from 5.04 GHz to 7.46 GHz, while the simulated result is from 5.04 GHz to 7.4 GHz. The measured  $|S_{11}| < -10$  dB impedance bandwidth of the RF antenna is from 5.96 GHz to 6.21 GHz, while the simulated result is from 6.13 GHz to

6.43 GHz. As for the AR character as shown in Fig. 20(b), both the simulated and measured curves of the RF and MS array antennas keep below the 3 dB, there are some points around the 5.1 GHz and 7.6 GHz in the measured results of MS antenna higher than the RF antenna for the asymmetrical structure of the MS unit. Compared with the simulated results, the measured curves shift to the higher frequency for the fabrication and measurement tolerance.

Figure 21 gives the radiation patterns compared with the reference antenna at 6.5 GHz and 7.2 GHz. At 6.5 GHz, the gain of the MS array antenna is improved by 4.94 dBi compared to the RF array antenna, the measured result is similar to the simulation. While compared with the RF antenna at 7.2 GHz, the gain is improved about 4.24 dBi, the side lobe of the measured left-hand radiation pattern has a little difference for the fabrication and measurement tolerance. Both antennas are left-hand CP radiating and the MS antenna possesses the characters of low side-lobe level and high radiation sufficiency.

As for verifying the scattering performance, the fabricated antennas was placed vertically on a foam platform in front of the two identical horn antennas with the measurement range of 1–18 GHz in the anechoic chamber as shown in Fig. 22. One horn antenna is used as transmitter while the other is for receiver to simulate the radar detecting devices. Figure 23 gives the measured RCS reduction of the MS antenna compared to the simulation results. The measured 6-dB reduction for the x-polarized of the MS antenna occurs from 4.88 to 11.63 GHz, which is in good agreement with the simulated results from 5.08 GHz to 11.46 GHz except for some frequency points. The difference mainly comes from the machining and measuring errors, but the results still confirm the effectiveness of the design.

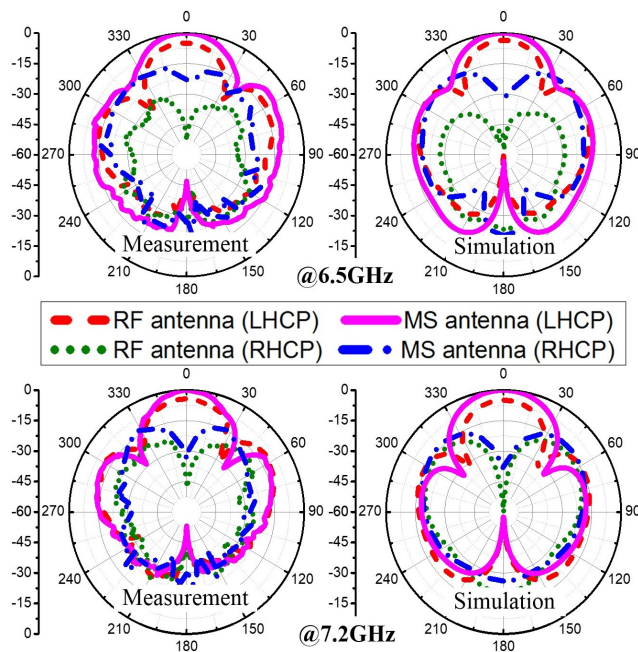


Fig. 21. Radiation patterns of the MS and RF array antennas.

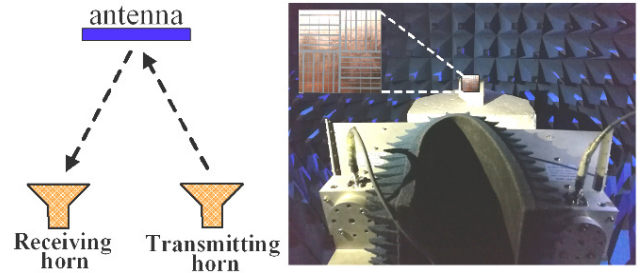


Fig. 22. The RCS measurement setup.

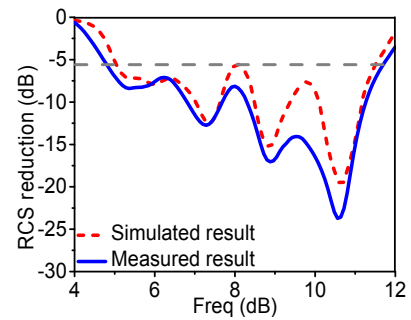


Fig. 23. The measured and simulated results of RCS-reduction.

Antenna	Radiation mode	Operation bandwidth	6dB RCS-reduction
[7]	Circular	10.74–12.33GHz (13.8%)	5–11.8GHz (80.8%)
[8]	Linear	10.74–12.33GHz (13.8)	4.2–10.6GHz (86.5%)
[17]	Circular	4.3–5.1GHz (17%)	4.53–6.70GHz (38.6%)
This paper	Circular	5.03–7.4GHz (38.1%)	5.08–11.46GHz (77.2%)

Tab. 3. Comparison of the proposed antenna with some similar works.

In order to clarify the effective design of the antenna in this paper, some similar works reported in the references are compared with the MS antenna array in Tab. 3. It can be concluded that both of radiation and scattering performance of the proposed antenna array in this paper have been significantly improved.

### 5. Conclusion

In this paper, a novel low-RCS wideband circularly polarized antenna array based on MS is designed. When illuminated by the radar detecting wave, the MS composed of the PDAMCs which are arranged like a chessboard can significantly bring the RCS down. While the compact structure of the MS and the driven patches allow the radiated electromagnetic wave propagate on the MS to generate additional resonances for widening the operation band and improving gain. Both the simulated and measured results indicate that the radar cross section (RCS) at bore-sight is reduced more than 6 dB from 5.08 GHz to 11.46 GHz except for some frequency points. The array antenna has a good broadside left-hand CP radiation, with the  $|S_{11}| < -10$  dB impedance bandwidth from 5.03 to

7.4 GHz and the 1-dB axial ratio bandwidth of 4–8 GHz. The MS antenna has a promising application in wideband wireless communication systems.

## Acknowledgments

This work was supported by the National Natural Science Foundation of China (no. 61471389, 61501494, 61671464 and 61701523), the Natural Science Foundational Research Fund of Shaanxi Province (no. 2017JM6025), and the Young Talent Fund of University Association for Science and Technology in Shaanxi, China (no. 20170107).

## References

- [1] YANG, F., RAHMAT-SAMII, Y. A low profile single dipole antenna radiating circularly polarized waves. *IEEE Transactions on Antennas and Propagation*, 2005, vol. 53, no. 9, p. 3083–3086. DOI: 10.1109/TAP.2005.854536
- [2] YI, H., QU, S. A novel dual-band circularly polarized antenna based on electromagnetic band-gap structure. *IEEE Antennas and Wireless Propagation Letters*, 2013, vol. 12, p. 1149–1252. DOI: 10.1109/LAWP.2013.2281060
- [3] YANG, W., TAM, K., CHOI, W., et al. Novel polarization rotation technique based on an artificial magnetic conductor and its application in a low-profile circular polarization antenna. *IEEE Transactions on Antennas and Propagation*, 2014, vol. 62, no. 12, p. 6206–6216. DOI: 10.1109/TAP.2014.2361130
- [4] CHUNG, K. High-performance circularly polarized antenna array using metamaterial-line based feed network. *IEEE Transactions on Antennas and Propagation*, 2013, vol. 61, no. 12, p. 6233–6237. DOI: 10.1109/TAP.2013.2282296
- [5] CHUNG, K., CHAIMOOL, S., ZHANG, C. Wideband subwavelength-profile circularly polarised array antenna using anisotropic metasurface. *Electronics Letters*, 2015, vol. 51, no. 18, p. 1403–1405. DOI: 10.1049/el.2015.2255
- [6] TA, S. X., PARK, I. Planar wideband circularly polarized metasurface-based antenna array. *Journal of Electromagnetic Waves and Applications*, 2016, vol. 30, no. 12, p. 1620–1630. DOI: 10.1080/09205071.2016.1210038
- [7] ZHENG, Y., GAO, J., CAO, X., et al. A broad-band gain improvement and wideband, wide angle low radar cross section microstrip antenna. *Acta Physica Sinica*, 2014, vol. 63, no. 22. DOI: 10.7498/aps.63.224102 (in Chinese)
- [8] CONG, L., FU, Q., CAO, X., et al. A novel circularly polarized patch antenna with low radar cross section and high-gain. *Acta Physica Sinica*, 2015, vol. 64, no. 22. DOI: 10.7498/aps.64.224219 (in Chinese)
- [9] ZHENG, Y., CAO, J., XU, L., et al. Ultra-wideband and polarization independent radar cross section reduction with composite artificial magnetic conductor surface. *IEEE Antenna and Wireless Propagation Letters*, 2017, vol. 16, p. 1651–1654. DOI: 10.1109/LAWP.2017.2660878
- [10] KANG, X., SU, J., ZHANG, H., et al. Ultra-wideband RCS reduction of microstrip antenna array by optimised multi-element metasurface. *Electronics Letters*, 2017, vol. 53, no. 8, p. 520–522. DOI: 10.1049/el.2017.0260
- [11] PAQUAY, M., IRIARTE, J., EDERRA, I., et al. Thin AMC structure for radar cross section reduction. *IEEE Transactions on Antennas and Propagation*, 2007, vol. 55, no. 12, p. 3630–3638. DOI: 10.1109/TAP.2007.910306
- [12] GAO, Q., YIN, Y., YAN, D., et al. Application of metamaterials to ultra-thin radar absorbing material design. *Electronics Letters*, 2005, vol. 41, no. 17, p. 936–937. DOI: 10.1049/el:20051239
- [13] LI, Y., ZHANG, H., FU, Y., et al. RCS reduction of ridged waveguide slot antenna array using EBG radar absorbing material. *IEEE Antennas and Wireless Propagation Letter*, 2008, vol. 7, p. 473–476. DOI: 10.1109/LAWP.2008.2001548
- [14] ZHOU, Y., CAO, X., GAO, J., et al. A C/X dual-band wide-angle reflective polarization rotation metasurface. *Radioengineering*, 2017, vol. 26, no. 3, p. 699–904. DOI: 10.13164/re.2017.0699
- [15] LI, S., CAO, X., GAO, J., et al. Fractal metamaterial absorber with three-order oblique cross dipole slot structure and its application for in-band RCS reduction of array antennas. *Radioengineering*, 2014, vol. 23, no. 4, p. 1048–1054.
- [16] LI, S., CAO, X., GAO, J., et al. Polarization-insensitive ultra-thin quasi-metasurface based on the spoof surface plasmon polaritons. *Applied Physics A: Materials Science and Processing*, 2016, vol. 122, no. 9, p. 1–9. DOI: 10.1007/s00339-016-0391-2
- [17] ZHAO, Y., CAO, X., GAO, J., et al. Broadband low-RCS circularly polarized array using metasurface-based element. *IEEE Antennas and Wireless Propagation Letters*, 2017, vol. 16, p. 1836–1839. DOI: 10.1109/LAWP.2017.2682848
- [18] PANG, Y., CHENG, H., ZHOU, Y., et al. Ultrathin and broadband high impedance surface absorbers based on metamaterial substrates. *Optics Express*, 2012, vol. 20, no. 11, p. 12515–12520. DOI: 10.1364/OE.20.012515
- [19] YANG, F., RAHMAT-SAMII, Y. Reflection phase characterization of the EBG ground plane for low profile wire antenna application. *IEEE Transactions on Antennas and Propagation*, 2003, vol. 51, no. 10, p. 2691–2703. DOI: 10.1109/TAP.2003.817559
- [20] YANG, F., RAHMAT-SAMII, Y. Polarization-dependent electromagnetic band gap (PDEBG) structures: designs and applications. *Microwave and Optical Technology Letters*, 2004, vol. 41, no. 6, p. 439–444. DOI: 10.1002/mop.20164
- [21] FOROOZESH, A., SHAFAI, L., NG MOU KEHN, M. Application of polarization and angular dependent artificial ground planes in compact planar high-gain antenna design. *Radio Science*, 2008, vol. 43, no. 6, p. 1–19. DOI: 10.1029/2007RS003795
- [22] HOSSEINIPANAH, M., WU, Q. Polarization-dependent artificial magnetic conductor structures using asymmetrical frequency selective surface. In *Proceedings of the 3rd IEEE International Symposium of Microwaves, Antennas, Propagation, EMC Technology, and Wireless Communication (MAPE)*. Oct. 2009, p. 707–710. DOI: 10.1109/MAPE.2009.5355646

## About the Authors...

**Xuewen ZHU** was born in Inner Mongolia province in 1995. He received the B.S. degree from the Air Force Engineering University in 2016. He currently works towards the M.S. degree at the Information and Navigation College. His research interests mainly include the electromagnetic metamaterial and metasurface antenna design.

**Jun GAO** received the B.Sc. and M.A.Sc. degrees from the Air Force Missile Institute in 1984 and 1987, respectively. He joined the Air Force Missile Institute in 1987 as

an assistant teacher. He became an associate professor in 2000. He is currently a professor of the Information and Navigation College, Air Force Engineering University of CPLA. He has authored and coauthored more than 100 technical journal articles and conference papers, and holds one China soft patent. His research interests include smart antennas, electromagnetic metamaterials and their antenna applications.

**Xiangyu CAO** received the B.Sc. and M.A.Sc. degrees from the Air Force Missile Institute in 1986 and 1989, respectively. She joined the Air Force Missile Institute in 1989 as an assistant teacher. She became an associate professor in 1996. She received Ph.D. degree from the Missile Institute of Air Force Engineering University in 1999. From 1999 to 2002, she was engaged in postdoctoral research in Xidian University, China. She was a Senior Research Associate in the Department of Electronic Engineering, City University of Hong Kong from Jun. 2002 to Dec. 2003. She is currently a professor of the Air Force Engineering University of CPLA. Her research interests include computational electromagnetic, smart antennas, electromagnetic metamaterial and their antenna applications, and electromagnetic compatibility.

**Tong LI** received the B.S. and Ph.D. degrees in Electronic and Information Engineering from Xidian University, Xi'an, China, in 2010 and 2015, respectively. She is currently a Lecturer with the Air Force Engineering University. Her current research interests include ultra-wideband

communication devices, reconfigurable antennas, and metasurface.

**Yuejun ZHENG** received the B.S. and M.S. degrees from the Air Force Engineering University (AFEU), Xi'an, China, in 2012 and 2014, respectively. He is currently pursuing the Ph.D. degree in Electromagnetic Field and Microwave Technology at the Information and Navigation Institute, Air Force Engineering University. His research interests include metasurface, metasurface antenna.

**Lili CONG** was born in Weihai Shandong province, P.R. China in 1991. She received B.S. and M.S. from the Air Force Engineering University, Xi'an China, in 2013 and 2015. She is currently working toward Ph.D. degree at the Information and Navigation College, Air Force Engineering University. Her main interests include metamaterial design and wideband RCS reduction.

**Liaori JI-DI** was born in Sichuan province, China. He received his B.S. degree from the Electronic and Information College, Tongji University in 2016. He currently works towards his M.S. degree. In his research, he specializes in metasurface, antenna array design and RCS reduction techniques.

**Bowen ZHU** was born in Inner Mongolia province in 1993. He received the B.S. degree from the Armed Police Engineering University in 2017. His research interests mainly include the electromagnetic metamaterial and metasurface antenna design.